Iris Recognition in the Visible Wavelength: Issues and Trends

Hugo Proença

Abstract The human iris supports contactless data acquisition and can be imaged covertly. Thus, at least theoretically, the subsequent biometric recognition procedure can be performed without subjects' knowledge. The feasibility of this type of recognition has received increasing attention and is of particular interest for forensic and security purposes, such as the pursuit of criminals and terrorists and the search for missing children. Among others, one active research area sought to use visible wavelength (VW) light imagery to acquire data at significantly larger distances than usual and on moving subjects, which is a difficult task because this *real-world* data is notoriously different from the one used in the near infra-red (NIR) setup. This chapter addresses the feasibility of performing reliable biometric recognition using VW data acquired under dynamic lighting conditions and unconstrained acquisition protocols: with subjects at large distances (between 4 and 8 meters) and on-the-move.

1 Introduction

The iris is known as one of the most valuable traits for the automatic identification of human beings and growing attention has been paid to the development of this technology [2]. A number of reasons justify this interest: (1) it is a naturally protected internal organ that is visible from the exterior; (2) it has a near circular and planar shape that turns easier its segmentation and parameterization and (3) its texture has a predominantly randotypic chaotic appearance that is stable over lifetime. The accuracy of the deployed iris recognition systems is remarkable: a study of 200 billion cross-comparisons conducted by Daugman [9] reported false acceptance rates of or-

Hugo Proença
University of Beira Interior, Department of Computer Science, IT- Instituto de Telecomunicações, 6201-001 Covilhã, Portugal. e-mail: hugomcp@di.ubi.pt

der 10^{-6} with false rejections of 1%. Other independent evaluations ([13] and [16]) confirmed these results.

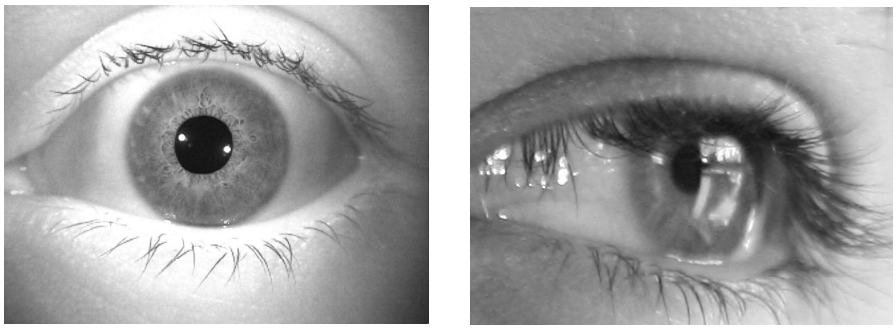

(a) *(b)*

Fig. 1 Comparison between (a) the quality of iris biometric images acquired in highly constrained conditions in the near-infrared wavelength (WVU database [25]) and (b) images acquired in the visible wavelength in unconstrained imaging conditions, acquired at-a-distance and on-the-move (UBIRIS.v2 database [24]).

However, currently deployed systems — that are based on Daugman's pioneering approach [6] — impose significant constraints on the subjects and acquisition environment, demanding that subjects stand relatively close and looking straight to the camera for several seconds while their eyes are illuminated by a near infra-red (NIR) source, enabling the capture of good quality data.

Why Use Visible Light?

Current systems require high illumination levels, sufficient to maximize the signal-to-noise ratio in the sensor and to capture images of the discriminating iris features with sufficient contrast. However, if similar processes were used to acquire iris images from a distance, acceptable depth-of-field values would demand significantly higher f-numbers for the optical system, corresponding directly (squared) with the amount of light required for the process. Similarly, the motion factor will demand very short exposure times, which again will require too high levels of light. The American and European standards councils ([1] and [5]) proposed safe irradiance limits for NIR illumination of near 10 mW / cm^2. In addition to other factors that determine imaging system safety (blue light, non-reciprocity and wavelength dependence), these limits should be taken into account, as excessively strong illumination can cause permanent eye damage. The NIR wavelength is particularly hazardous, because the eye does not instinctively respond with its natural mechanisms (aversion, blinking and pupil contraction). However, the use of visible light and un-

constrained imaging setups can severely degrade the quality of the captured data (figure 1), increasing the challenges in performing reliable recognition.

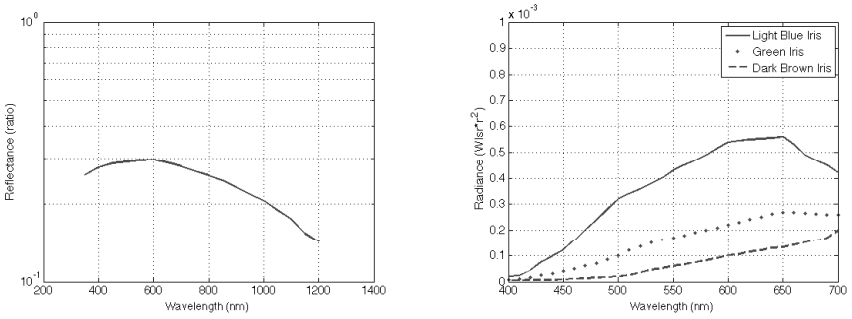

(a) *(b)*

Fig. 2 Spectral reflectance and radiance of the iris and the sclera in respect of the wavelength. Spectral reflectance of the human sclera [22]. Spectral radiance of the human iris according to the levels of iris pigmentation [14].

The pigmentation of the human iris consists mainly of two molecules: brown-black Eumelanin (over 90%) and yellow-reddish Pheomelanin [18]. Eumelanin has most of its radiative fluorescence under the VW, which—if properly imaged—enables the capture of a much higher level of detail, but also of many more noisy artifacts, including specular and diffuse reflections and shadows. Also, the spectral reflectance of the sclera is significantly higher in the VW than in the NIR (figure 2a) and the spectral radiance of the iris in respect of the levels of its pigmentation varies much more significantly in the VW than in the NIR (figure 2b). These optical properties are the biological roots behind the higher heterogeneity of the VW iris images, when compared with the traditional NIR data. Also, the types and number of noisy artifacts likely to appear in VW and NIR data are notoriously different, which justify the need to specialized recognition strategies.

The feassibility of the unconstrained VW iris recognition remains controversial, and several skepticisms remain, specialy for high pigmented irises that constitute the majority of the world's population. This chapter has two major parts: (1) to describe a data set of VW iris images captured in unconstrained conditions and (2) to discuss the major issues for VW iris recognition, namelly describing the factors that likely degrade performance and giving results about the specificity and sensitivity that pattten recognition (PR) systems achieve in such challenging conditions.

2 Less Constrained Iris Recognition

The term *constraint* refers to one of the factors that currently deployed systems impose, in order to perform recognition with enough confidence: subjects distance, motion and gaze direction and lighting conditions of the environment. These constraints motivate growing research efforts and became the focus of many recent proposals, among which the "Iris-on-the-move" project [17] should be highlighted: it is a major example of engineering an image acquisition system to make the recognition process less intrusive for subjects. The goal is to acquire NIR close-up iris images as a subject walks at normal speed through an access control point. *Honeywell Technologies* applied for a patent [12] on a very similar system, which was also able to recognize irises at a distance. Previously, Fancourt *et* al. [10] concluded that it is possible to acquire sufficiently high-quality images at a distance of up to ten meters. Narayanswamy and Silveira [21] used a wavefront coded optic to deliberately blur images in such a way that they do not change over a large depth-of-field. Removing the blur with digital image processing techniques makes the trade-off between signal-to-noise ratio and depth of field linear. Also, using wavefront coding technology, Smith *et* al. [26] examined the iris information that could be captured in the NIR and VW spectra, addressing the possibility of using these multispectral data to improve recognition performance. Park and Kim [23] acquired in-focus iris images quickly at a distance, and Boddeti and Kumar [3] suggested extending the depth-of-field of iris imaging frameworks by using correlation filters. He *et* al. [11] analyzed the role of different NIR wavelengths in determining error rates. More recently, Yoon *et* al. [28] presented an imaging framework that can acquire NIR iris images at-a-distance of up to three meters, based on a face detection module and on a light-stripe laser device used to point the camera at the proper scene region. Boyce *et* al. [4] studied the image acquisition wavelength of revealed components of the iris, and identified the important role of iris pigmentation. Although concluding that illumination inside the 700-900 nm optimally reveals the richness of the iris structure, they observed that irises with moderate levels of pigmentation could be imaged in the visible light with good quality.

3 The UBIRIS.v2: A Database of Visible Wavelength Iris Images Captured On-The-Move and At-A-Distance

As described in [24], the major purpose of the UBIRIS.v2 data set is to constitute a new tool to evaluate the feasibility of visible wavelength iris recognition under far from ideal imaging conditions. The various types of non-ideal images, imaging distances, subject perspectives and lighting conditions existent on this database could be of strong utility in the specification of the visible wavelength iris recognition feasibility and constraints.

Image Acquisition Framework and Set-Up		
Camera = Canon EOS 5D	Color Representation = sRGB	Shutter Speed = 1/197 sec.
Lens Aperture = F/6.4 - F/7	Focal Length = 400 mm	F-Number = F/6.3 - F/7.1
Exposure Time = 1/200 sec.	ISO Speed = ISO-1600	Metering Mode = Pattern
Details of the Manually Cropped Resultant Images		
Width = 800 pixels	Height = 600 pixels	Format = tiff
Horizontal Resolution = 72 dpi	Vertical Resolution = 72 dpi	Bit Depth = 24 bit
Volunteers		
Totals = Subjects 261; Irises 522; Images 11 102		
Gender = Male: 54.4%; Female: 45.6%		
Age = [0,20]: 6.6%; [21,25]: 32.9%; [26,30]: 23.8%; [31,35]: 21.0%; [36,∞[: 15.7%		
Iris Pigmentation = Light : 18.3%; Medium : 42.6%; Heavy : 39.1%		

Table 1 Details of the UBIRIS.v2 images, of the image acquisition framework and set-up and of the subjects that offered themselves as volunteers to the imaging sessions.

The setup of the used imaging framework is given in table 1. This framework was installed on a lounge under both natural and artificial lighting sources. Several marks were placed on the floor (between three and ten meters away from the acquisition device) and asked for volunteers for the image acquisition processes. Two distinct image acquisition sessions were performed separated by an interval of one week. From the first to the second session the location and orientation of the acquisition device and artificial light sources was changed, in order to increase heterogeneity. Volunteers were at large majority latin caucasian (around 90%) and also black (8%) and asian people (2%). Around 60% of the volunteers performed both imaging sessions, while 40% performed exclusively one, either during the first or second acquisition period.

Subjects were required to walk toward the acquisition device and look at several lateral marks that obliged them to rotate head and eyes, enabling the manual capturing of 3 images per meter, between eight and four meters, giving a total of 15 images per eye and session. As it is illustrated in figure 3, the used acquisition setup and protocol enabled to acquire sequences of iris images with different scale, gaze and under different types of illumination for each subject. The used acquisition hardware and setup (Table 1) enables the capturing of iris data with dimensions that in most cases is compliant with the standard for iris images (ISO/IEC, 2004) that recommends a minimum of 100 and preferable 200 pixels across the iris diameter.

A varying number of subjects offered as volunteers for the first, second or for both imaging sessions. However, assuming that each iris image can be used to generate a biometric template, that the other images from the same eye can be used to assess *match* variability and all the remaining images can be used to assess *non-match* variability, it is possible to obtain a bound for the error that is possible to be tested with statistical significance.

The 11 102 images of the UBIRIS.v2 database enable respectively 127 746 match and 61 482 804 non-match comparisons. This guarantees statistical significance in

Fig. 3 Examples of close-up iris images acquired at different distances (between eight at the far left and four meters at the far right), on a continuously moving subject and under dynamic lighting conditions.

experiments with an empirical error rate $\hat{P}$ down to $1,623 \times 10^{-6}\%$. However, this value should be regarded as a lower bound, substantially increased the independence between images is not assumed and error correlations are taken into account.

4 Less Constraining Acquisition Frameworks

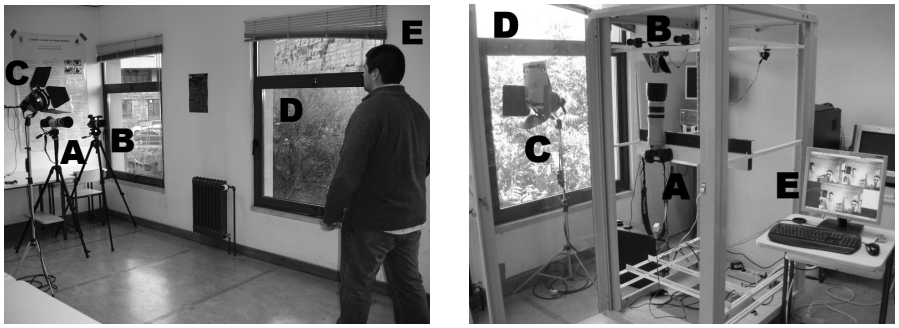

(a) *(b)*

Fig. 4 Overview of the image acquisition frameworks (a) used in collecting the UBIRIS.v2 data set (A,B), light sources (C,D) and subjects location (E) and (b) used to automatically perform image acquisition, with labels similar to the manual configuration.

Figure 4a gives a global perspective of the used acquisition framework and of the environment where data of the UBIRIS.v2 database was collected. In order to disburden the imaging sessions for volunteers and maximize the number of usable images per subject, we decided to perform data acquisition manually. However, a completely automated process could have been performed, using state-of-the-art techniques of human silhouette and face detection and object tracking.

In the meanwhile, a completely automated acquisition framework was devised, being composed by two commercial web cameras, a pan-and-tilt device and the

same high resolution camera as before (figure 4b). The process starts by a software module that performs the detection of human silhouettes, according to the data acquired from one of the web cameras. Using this information and a set of semantic rules, a region of the scene is cropped and given to the real time face detector module (according to the well known method of Viola and Jones [27]). This phase given the 2D position (x,y) of a face in the scene, which is then sent to a stereo vision module that collects data from both web cameras and infer the subject depth in the scene, i.e., the distance z between the acquisition camera and the subject. Using the pan-and-tilt device, the acquisition camera is directed to the 3D scene point at coordinates (x,y,z) and an image that contains approximately the region of the subject's head is captured. Finally, using a set of biologically-based semantic rules, a region that contains the subject's eyes is cropped and used in the biometric recognition phases.

Such a completely automated framework would be continuously acquiring and processing data without any human supervision, which increases probability for the acquisition of extremely degraded data: images might be completely out-of-focus due to exaggerated movements, might be captured under unusable perspectives due to subjects gaze and even out-of-iris images are probable due to failures in the human silhouette and face detection modules. Due to these probabilities, image quality assessment is fundamental and have as goal to quantify characteristics and fidelity of the segmented data, particularly in terms of its utility. Such assessment module should act as a filter for most of the acquired data and select the key frames that are more likely to be conveniently handled by the later recognition modules.

4.1 Image Assessments

The error rates of any biometric system mainly depend on the amount of information captured, as well n the proportion of noise that obstructs the underlying texture and corrupts the discriminating information.

In order to establish a relationship between the image acquisition distance and the maximum amount of iris data that is possible to capture with the described image acquisition framework and setup, the average iris diameter of frontal images was measured, with respect to the acquisition distance. The obtained results are given in figure 5a and indicate that the diameter of the captured irises varies according to an inverse logarithmic function. Through trial-and-error interpolation, the following coarse approximation function $d(x) : \mathbb{R}^+ \rightarrow \mathbb{R}^+$ was obtained:

$$d(x) \approx \frac{150}{ln(\frac{x}{1.85})} \tag{1}$$

where x is the image acquisition distance (meters) and $d(x)$ is the average diameter of the captured irises. This is confirmed in figure 5b, that gives the images resolution in the iris regions, where the shaded areas represent the 95% confidence intervals. Results were obtained through the division of the number of pixels that

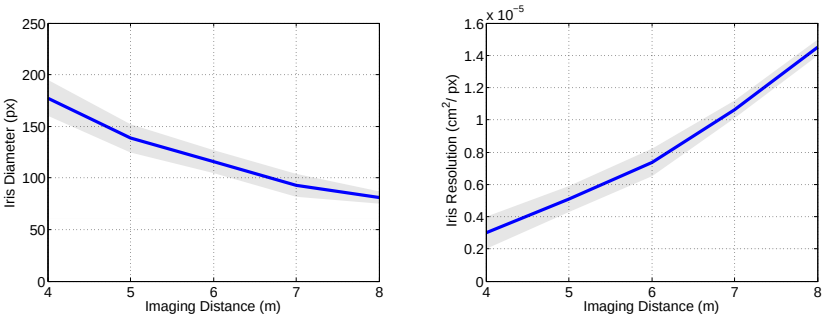

(a) *Average diameters of the captured irises as a function of the image acquisition distance.*

(b) *Average images resolution at the iris regions, as a function of the image acquisition distance.*

Fig. 5 Maximum amount of information possible to acquire at-a-distance and on-the-move through the used image acquisition framework and setup.

fall into the iris region by an iris area of 0.785 cm^2, averaged from human eye's morphology studies that are publicly available. These observations confirm that the afore described acquisition framework and setup enables the capturing of sufficient data to perform iris recognition, as near 50% of the database images have iris diameters close to the lower bound (140 pixels) recently proposed by Daugman [7].

The proportion of iris pixels that are occluded was obtained and results are shown in the histogram of figure 6a. The horizontal axis denotes the proportion of noise-free pixels and the vertical axis the respective probability of occurrence in the database. It was observed that - on average - 25-30% of the pixels that fall within the iris ring were corrupted by one of the local noise factors. Also, just about 3% of the images are completely noise-free, while around 0.9% contain full noisy data, correspondent to out-of-iris images or imaged in extremely poor lighting conditions.

Images texture was assessed by means of the *image entropy*, a statistical randomness measure widely used in the image processing domain. According to the conclusion reported by He *et* al. [11], we considered the levels of iris pigmentation as a factor that influences the amount of discriminating information captured for biometric purposes.

Let I be a grayscale image with g gray levels, and $p(k)$ be the probability of occurrence of the gray level k in I. The image entropy h is given by $h(I) = -\sum_0^{g-1} p(k)\ log_2(p(k))$. Let B be the binary noise mask that gives the non-occludded iris regions of I. Thus, $B(x,y) = 0$ or 1 when the respective pixel (x,y) respectively belongs to the iris ring and is noise-free or not. The *entropy of the iris region* $ih(.)$ of I was obtained taking exclusively into account pixels (x_i,y_i) such that $B(x_i,y_i) = 0$, i.e., the noise-free iris data. Finally, for normalization purposes, the entropy value was divided by the area of the noise-free iris region

$$ih(I) = \frac{h(I(x,y)|B(x,y)=0)}{\mathbb{I}_{\{B(x,y)=0\}}} \quad (2)$$

where $\mathbb{I}_{\{.\}}$ is the characteristic function.

The obtained values are given in figure 6b. The horizontal axis corresponds to the imaging distance and the vertical axis to the entropy value. Data points give the observation average values for *light* (continuous series), *medium* (dotted series) and *heavy* pigmented irises (dashed series), as a function of the imaging distance. The shaded areas represent the 95% confidence intervals. It can be confirmed that the average entropy of the iris data decreases inversely with the imaging distance and, more evidently, with the levels of iris pigmentation.

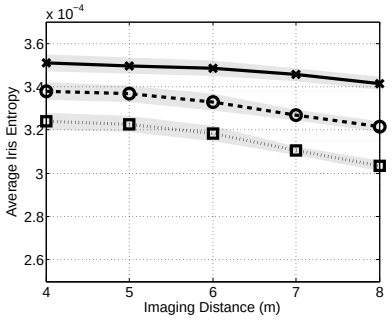

(a) *Proportion ([0,1]) of noise-free iris data within the captured iris rings.*

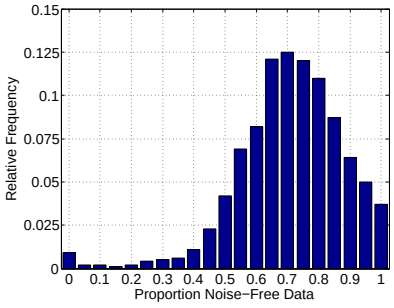

(b) *Average image entropy of the noise-free iris regions.*

Fig. 6 Proportion of noise that occludes the iris texture (figure 6a) and average entropy of the noise-free iris regions as function of the levels of iris pigmentation (figure 6b). Light, medium and heavy pigmented irises are represented by the continuous, dotted and dashed lines.

4.2 Degradation Factors

Images of the UBIRIS.v2 data set are degraded by several factors and are high heterogeneous, regarding the lighting conditions of the environment. Through visual inspection, fourteen different factors were detected and classified into one of two major categories: *local* or *global*, as they affect exclusively image regions or the complete image. The *local* category comprises iris obstructions, reflections, off-angle and partial images, while the *global* comprises poor focused, motion-blurred, rotated, improper lighting and out-of-iris images. Examples of the UBIRIS.v2 noise factors are given in figure 7.

(a) *Good quality iris image.*

(b) *Off-angle iris image.*

(c) *Poor focused iris image.*

(d) *Rotated iris image.*

(e) *Motion-blurred iris image.*

(f) *Iris obstructions due to eyelids.*

(g) *Iris obstructions due to eyelashes.*

(h) *Iris obstructions due to glasses.*

(i) *Iris obstructions due to contact lenses.*

(j) *Iris obstructions due to hair.*

(k) *Iris imaging in poor lighting conditions.*

(l) *Iris with specular reflections.*

(m) *Iris with lighting reflections.*

(n) *Partial captured iris.*

(o) *Out-of-iris image.*

Fig. 7 Comparison between a good quality image (figure 7a) and several types of non-ideal images of the UBIRIS.v2 database. These images resulted of less constrained imaging conditions, under varying lighting conditions, at-a-distance and on-the-move subjects.

4.3 Specificity

Several works about the iris recognition technology reported a very small - almost infinitesimal - probability of produce a false match in the comparison between signatures extracted from data with good quality (e.g., [7], [15], [13] and [16]). This is due to the chaotic appearance of the main components of the iris texture and is regarded as one of the technology's major advantages, when compared to other bio-

metric traits. Also, this is of specially interest for the type of recognition discussed in this paper: to guarantee that the comparison between templates (extracted from good quality data) and samples extracted from degraded iris data (or even from partial or non-iris regions due to failures on the eye detection and segmentation modules), will not frequently produce false matches.

This hypothesis was tested through a procedure illustrated in figure 8. Using the recognition method proposed by Daugman [7] - composed by iris segmentation, normalization (Daugman Rubber Sheet), encoding (bidimensional Gabor wavelets) and matching (Hamming distance) - we extracted 1 000 signatures from UBIRIS.v2 iris images with good quality. Further, we extracted a set of sample signatures from 1 000 iris images with very poor quality, 10 000 non-iris or partial iris images and 10 000 natural and synthetic textures images. Finally, we performed a '*one against all* comparison between each template and the set of samples, giving a total of 21 000 000 comparisons. During these tests we didn't get a single dissimilarity value close to the usual acceptance threshold (0.33), which means that not even a single false acceptance was observed if the traditional acceptance thresholds are used.

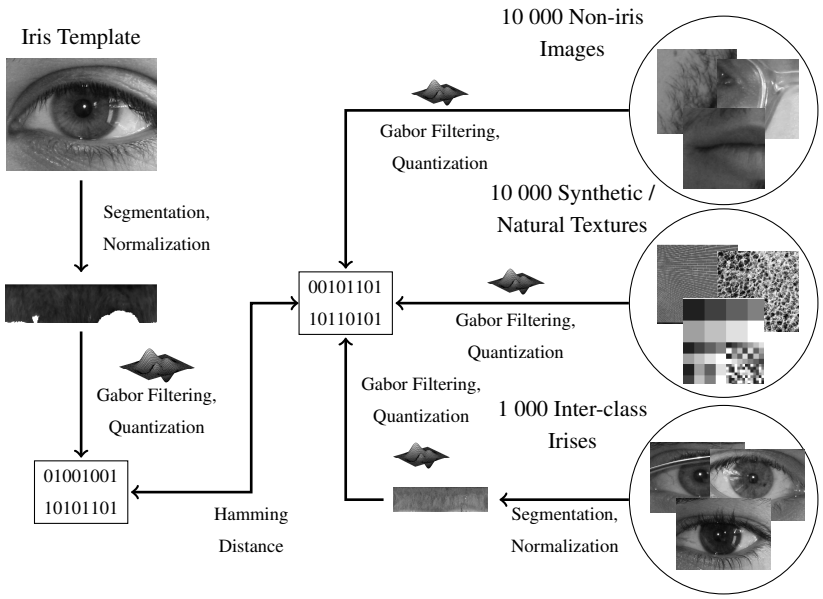

Fig. 8 Setup of the experiments performed to evaluate the probability of produce a false match in the comparison between iris signatures extracted from good quality data ("iris template") and signature samples resultant from iris data with bad quality, or even partial or non-iris data. We used the main recognition stages proposed by Daugman and successfully deployed in recognition systems to evaluate the probability of produce a false match in these situations.

Figure 9 gives the histogram of the obtained dissimilarity values (vertical bars) and the approximated Gaussian distribution (line plot with $\mu = 0.49992$ and $\sigma = 0.02419$). We confirmed that, even on high degraded data, the used iris encoding and comparison strategies produce a false match with almost null probability. Based on the parameters of the fitted Gaussian distribution, the probability of producing a dissimilarity value lower than 0.33 will be approximately of 1.03923×10^{-12}. Once again, the role of this value for the type of recognition discussed in this paper should be stressed: it can be assumed with extreme high confidence that such recognition systems will not produce false matches and, thus, any match reported has a full probability of being genuine. This means that, independently of how much false rejections will be frequent (due to lighting variations, movements and gazes) any reported match is high reliable.

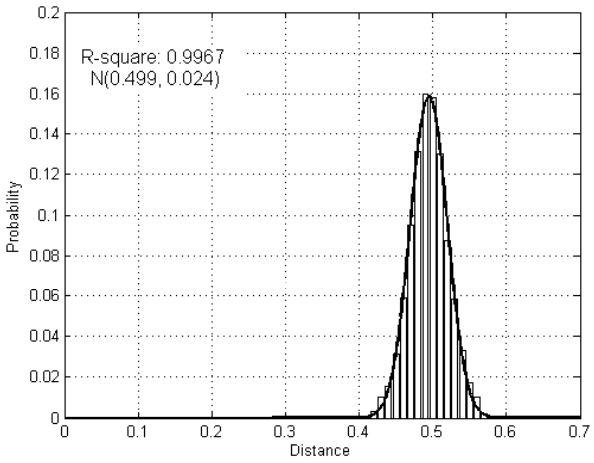

Fig. 9 Histogram of the obtained dissimilarities when comparing signatures extracted from 1 000 templates with good quality and 21 000 signatures extracted from iris images with bad quality, partial irises and non-iris data. "R-square" gives the goodness-of-fit of the plotted Gaussian distribution with $\mu = 0.499$ and $\sigma = 0.024$ to the obtained results.

4.4 Sensitivity

As expected, the uncontrolled imaging conditions and acquisition setups lead to data with notoriously heterogeneous quality, which will have evident impact in the recognition rates of VW iris biometric systems. In this scope, quality assessment is a fundamental task. The goal is to quantify characteristics and fidelity of the segmented data, particularly in terms of its utility. This is essential, as performing recognition in

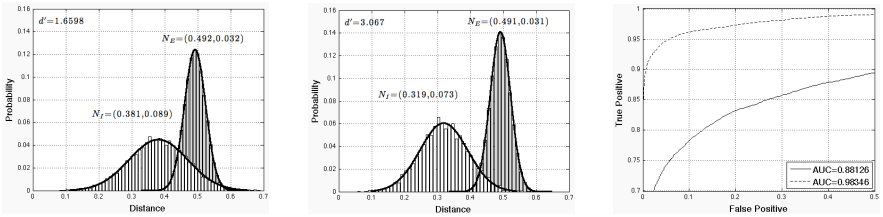

(a) *(b)* *(c)*

Fig. 10 Comparison between the histograms of the fractional Hamming distances obtained (a) for a sub-set of 10 427 images of the UBIRIS.v2 database and (b) when samples of poor quality are not considered to the recognition test. Figure at far right gives the corresponding Receiver Operating Characteristic curves.

too much degraded data decreases matching accuracy and increases computational complexity.

According to the afore observations, this section aims at give an approximation of the recognition rate that VW iris recognition systems can achieve, according to data quality. For such, we used the classical Daugman's recognition strategy [7], as it is the most well known and is functioning in the large majority of the commercially deployed systems. According to this choice, the segmented boundaries were normalized to dimensionless polar coordinates. Then, a bank of Gabor filters was used to analyze the iris texture and the angle of each phasor quantized to one of four quadrants. Finally, the fractional Hamming distance gave the dissimilarity between two irises. A subset of 10 427 UBIRIS.v2 images was selected, which under visual inspection we verified that the segmentation method has accurately segmented. Then, for all subsequent experiments this set was divided according to different criteria. For comprehensibility, we refer to a *recognition test* when each sample of a data set is matched against all the remaining images of the the same data set, resulting in two types of comparisons: intra-class (match) and inter-class (non-match). As suggested by Daugman [8], for two-choice decisions the decidability index d' measures how well separated are the two types of distributions and recognition errors correspond to their overlap area:

$$d' = \frac{|\mu_E - \mu_I|}{\sqrt{\frac{1}{2}(\sigma_I^2 + \sigma_E^2)}} \tag{3}$$

where μ_I and μ_E are the means of the two distributions and σ_I and σ_E their standard deviations.

Figure 10 compares the histograms of the fractional Hamming distances for the match (light bars) and non-match (dark bars) comparisons obtained when all images were used in the recognition test (figure at the far left) and when the poorest quality samples (according to the visual perception of quality) were rejected (figure at the

center). The line plots correspond to the fitted Normal distributions and the upper left corner gives the corresponding decidability index d'. As general considerations, we confirmed that values obtained for the non-match distributions do not significantly vary according to the quality of the data and are almost the same reported for the NIR constrained recognition setups. Oppositely, there is a significant movement of the match distributions toward the non-matches, substantially decreasing the sensitivity of the system, if traditional acceptance thresholds are used. Due to this, the decidability of the VW recognition systems significantly varied. Figure 10c shows how the true and false matches in our system would change according to different decision thresholds, when no quality is considered (continuous line) and when only samples with good quality are considered for recognition (dashed line). Here, we plot the area under curve (AUC) for both setups, which significantly augments as the poorest quality samples are rejected.

The next question to consider is about the effect of each factor in the effectiveness of VW iris recognition systems, specially in its sensitivity. For such, we repeated the "one-against-all" recognition setup, but selecting several sub-sets, each one containing samples that are notoriously degraded by each analyzed factor: scale, focus, gaze and levels of iris pigmentation. It should be noted that although this experiment enables to perceive *how much* recognition effectiveness is degraded by each factor, it cannot be regarded as an effective evaluation. This will demand a data set with images degraded exclusively by one factor and UBIRIS.v2 images (as well all the remaining available data sets) are simultaneously degraded by various factors.

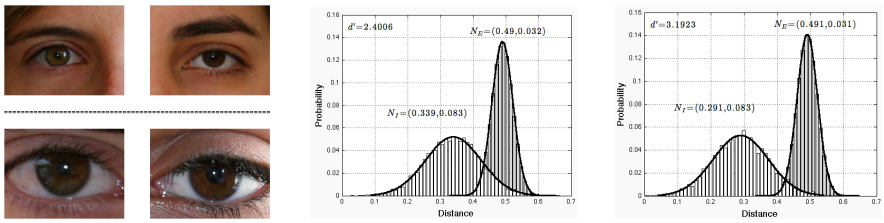

(a) *(b)* *(c)*

Fig. 11 UBIRIS.v2 images contains images captured at notoriously different scales, between 4 and 8 meters (a). Figures at the center and far right compares the match and non-match histograms of the fractional Hamming distances obtained for images captured at the farthest (b) and closest (c) scales.

The initial evaluation is about the effect of scale in the recognition sensitivity (figure 11). For such, two sub-sets with good quality images that were acquired at the farthest (8 meters) and closest (4 meters) distances were selected. Under visual inspection, the quality of each image was verified, having as main concern to exclusively select focused images with practically un-occluded irises and gaze aligned with the optical axis of the camera. Figure 11 shows how the histograms of the match

and non-match distributions would change according to the scale criterium. The observed values for the non-match distributions remained approximately equal, in opposition with the match distributions that appears to move toward the non-matches, as the acquisition distance augments. This is probably due to the ?? Justificacao Matey??.

Then, we assessed the impact that levels of image focus could have in the sensitivity of VW recognition systems. A subset composed by good quality images was selected, composed by focused images with occluded irises and gaze aligned with the optical axis of the camera. As defocus is equivalent to multiplying the 2D Fourier transform of a perfectly focused image by a 2D Fourier transform of a Gaussian kernel, an artificial set of defocused images was obtained by the convolution with the previous images with a Gaussian kernel of width 5 and σ 2.0. As expected, we observed a relatively minor impact of focus in recognition effectiveness (figure 12), as it is known that most of the iris discriminating information spans between 2 and 3 octaves of the original scale and only severe defocus would notoriously affect the recognition process. In our opinion this is one of the biggest advantages of the iris, when compared to other biometric traits: using the lowest and middle-low frequency components for recognition improves the robustness to noise (focus and artifacts) in less constrained acquisition setups.

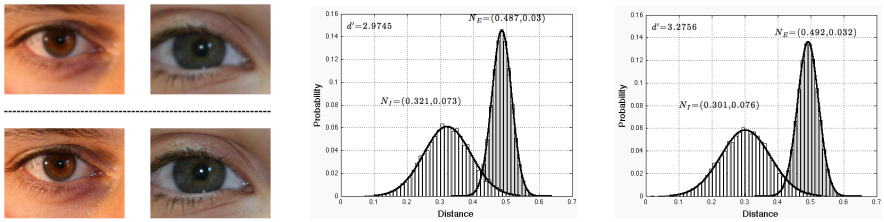

(a) *(b)* *(c)*

Fig. 12 The acquisition of a small moving target (iris) at relatively large distances propitiates very different levels of image focus (a). Figures at the center and far right compares the match and non-match histograms of the fractional Hamming distances obtained for blurred (b) and focused (c) images.

Due to the intrinsic properties of the used iris encoding and matching strategies, it is expected that variations in subjects gaze may have big influence in recognition effectiveness, when compared to other factors. We suspect that gaze propitiates significant perspective deformations in the iris texture and these cause significant changes in phase, deteriorating the recognition effectiveness. This is reiterated in figure 13 that compares the results obtained when the recognition tests were performed on images that under visual inspection were considered as aligned and another set that contains images with moderate to severe deviations between the subjects gaze and the optical axis of the camera.

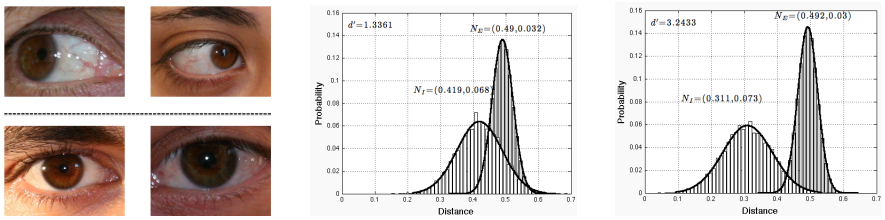

(a) *(b)* *(c)*

Fig. 13 Acquiring data from moving subjects and without requiring them any type of cooperation increases the probability of capturing off-angle irises, when the subject's gaze is not aligned with the optical axis of the camera (a). These variations cause perspective deformations in the iris texture and significant changes in phase. Taking into account that current state-of-the-art techniques are phase-based, this may lead to significant deteriorations in the recognition effectiveness, as it is illustrated by the results given in (b) off-angle images and (c) aligned images.

As stated before, most of the skepticism in the development of iris recognition systems that operate in the VW is for high pigmented irises, corresponding to dark brown and almost black perceived colors, with a very low albeldo. While they constitute the large majority of the world population, it is considered that these irises would demand very strong light sources, in order to be acquired with sufficient discriminating information. Here, we infer *how much* the levels of iris pigmentation increase the recognition challenges, by analyzing the separability between intra-class and inter-class comparisons obtained for two subsets of good quality images (focused, without significant occlusions or gaze deviations) with very different levels of iris pigmentation. The "light" subset contains light pigmented irises, corresponding to blue and light green eyes. The "dark" subset is composed by dark brown and black irises and includes almost all the images of the African and Asian volunteers of the UBIRIS.v2 data set. Figure 14 confirms that the levels of iris pigmentation constitute an obstacle to VW iris recognition, as the decidability values obtained for light pigmented irises (right histograms) were notoriously higher than those obtained when heavily pigmented images were used. The justification for these result lies in the spectral absorbance of the predominant pigment of the human iris (brown-black Eumelanin), that has a peak in the VW. Thus, the levels of iris pigmentation are in direct proportion of the tissue absorbance and inverse to the perceived albeldo, which turns more difficult to capture the discriminating patterns of heavily pigmented irises (ridges, valleys, furrows and crypts).

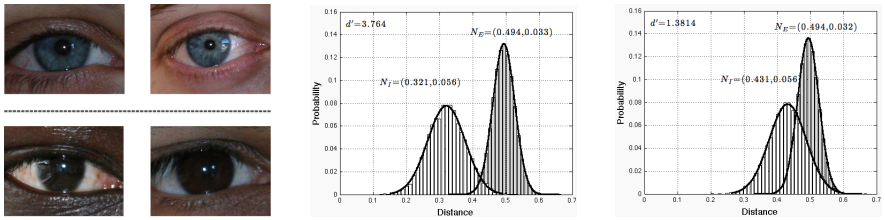

(a) *(b)* *(c)*

Fig. 14 The spectral absorbance of the human iris predominant pigment (Eumelanin) has a peak in the VW, which turns more difficult to capture the discriminating patterns of high pigmented irises. This is confirmed by the reduced separability between the intra-class and inter-class comparisons obtained for high pigmented irises (c) when compared with the results obtained for light pigmented ones (b).

5 Conclusions and Trends

The possibility of performing automatic recognition of human beings in uncontrolled environments and without requiring them any type of cooperation is of evident interest or forensic and security purposes and represents a *grand-challenge* for the pattern recognition community. To the best of our knowledge, no method was developed to achieve such purpose, which will have effective consequences in the everyday style of modern societies.

This chapter addressed the use of VW light to perform iris biometric recognition in scenarios that are far less constrained than those where currently deployed systems are operating with success: at larger image acquisition ranges (between 4 and 10 meters) and on moving subjects. As expected, the acquired *real world* data brings many challenges to the pattern recognition task, as it might be degraded by several factors and contains various types of noise artifacts that obstruct the discriminating iris texture and difficult the recognition process.

We start by presenting the main characteristics of a data set that is free available for the research community (UBIRIS.v2), that can provide a common comparison term for the fair comparisons between different proposals.

The optical properties of the iris, namely its spectral absorbance and reflectance, was overviewed in order to give an idea of the major discriminating points between the appearance of data acquired in the well known NIR scenario and in the VW. Special attention was paid to the factors that are likely to degrade the effectiveness of VW iris recognition systems and motivated serious skepticism about the possibility of performing reliable recognition in such challenging conditions. Even so, preliminary experiments appear to confirm that this task is possible, which is justified by two reasons: (1) an extremely low probability for the existence of false acceptances was observed, even when using the same recognition strategies used for NIR data and (2) the observed sensitivity of recognition systems in such data, which points

that an evident amount of information that discriminates between different subjects is able to be acquired in the described conditions and used for recognition purposes.

Due to the extremely appealing potential applications of these systems, a growing number of researchers are working on this field and proposing specialized strategies to perform the automatic acquisition, segmentation, normalization and encoding and matching of real world VW data. Among them, there is an extremely promising new type of biometric recognition called *periocular biometrics* that refers to the regions in the immediate vicinity of the eye (figure 15) and attempts to perform recognition based not only in the iris but also to its neighborhood.

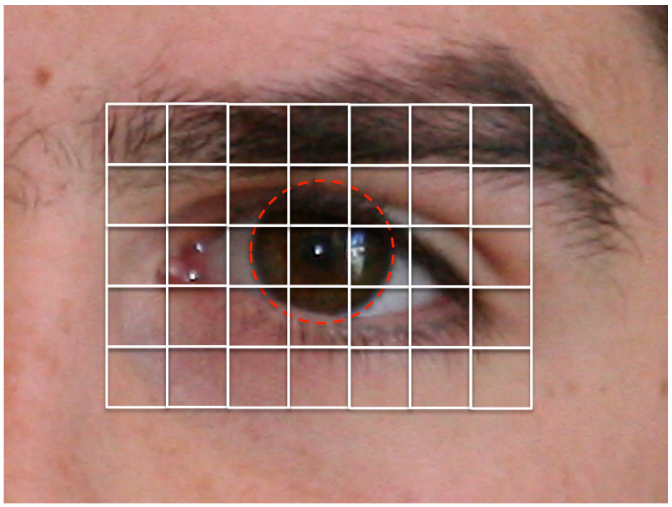

Fig. 15 Periocular biometrics refers to the automatic recognition of human beings using not only the information of the iris texture but also of the surrounding information (eyelids, eyelashes, skin, eyebrow). This type of recognition can provide a significant improvement toward the development of recognition methods that perform surreptitiously and in unconstrained environments.

As argued by [20] and [19], periocular recognition is a trade-off between using the entire face region or only the iris: it avoids the resolution problems of iris images captured at large distances and can be used for a wide range of distances. Also, face images acquired from unconstrained environments often suffer from poor illumination, motion blur, low resolution and pose variations. that significantly degrade the effectiveness of face recognition techniques. To the best of our knowledge, few studies have been conducted on the use of the periocular region as a biometric trait. Park et al. [20] used both local and global image features to match periocular images acquired with visible light and established its utility as a soft biometric trait. Also, Miller et al. [19] used Local Binary Pattern (LBP) to encode and match periocular images.

Acknowledgements The financial support given by "FCT-Fundação para a Ciência e Tecnologia" and "FEDER" in the scope of the PTDC/EIA-EIA/103945/2008 ("NECOVID: Negative Covert Biometric Identification") research project is acknowledged.

References

1. American National Standards Institute. American national standard for the safe use of lasers and LEDs used in optical fiber transmission systems, ANSI Z136.2 (1988)
2. Bowyer K., Hollingsworth K., Flynn P.: Image understanding for iris biometrics: A survey. Computer Vision and Image Understanding. **110**, 2 , 281–307 (2008)
3. Boyce C., Ross A., Monaco M., Hornak L., Li X.: Multispectral iris analysis: A preliminary study. In *Proceedings of the First IEEE International Conference on Biometrics: Theory, Applications, and Systems*. 1–8, U.S.A (2008)
4. Boddeti N., Kumar V.: Extended depth of field iris recognition with correlation filters. In *Proceedings of Computer Vision and Pattern Recognition Workshop on Biometrics*, 51–59, U.S.A. (2006)
5. Commission International de l'Eclarirage. Photobiological safety standards for safety standards for lamps. Report of TC 6-38, CIE 134-3-99 (1999)
6. Daugman J.: High confidence visual recognition of persons by a test of statistical independence. IEEE Transactions on Pattern Analysis and Machine Intelligence, **25**, 11, 1148–1161, U.S.A. (1993)
7. Daugman J.: How iris recognition works. IEEE Transactions on Circuits and Systems for Video Technology. **14**, 1, 21–30 (2004)
8. Daugman J.: Biometric Decision Landscapes. Tech Report TR482, `http://www.cl.cam.ac.uk/users/jgd1000/biomdecis.ps` (2000)
9. Daugman J.: Probing the Uniqueness and Randomness of IrisCodes: Results From 200 Billion Iris Pair Comparisons . Proceedings of the IEEE, **94**, 11, 1927–1935, U.S.A. (2006)
10. Fancourt C., Bogoni L., Hanna K., Guo Y., Wildes R., Takahashi N., Jain U.: Iris recognition at a distance. In *Proceedings of the 2005 IAPR Conference on Audio and Video Based Biometric Person Authentication*, 1–13, U.S.A. (2005)
11. He Y., Cui J.,Tan T., Wang Y.: Key techniques and methods for imaging iris in focus. In *Proceedings of the IEEE International Conference on Pattern Recognition*, 557–561, Hong Kong (2006)
12. Honeywell International Inc.: A distance iris recognition. United States Patent 20070036397 (2007)
13. International Biometric Group: Independent test of iris recognition technology, `http://www.biometricgroup.com/reports` (2005)
14. Imai F.: Preliminary experiment for spectral reflectance estimation of human iris using a digital camera. Technical report, Munsell Color Science Laboratories, Rochester Institute of Technology (2000)
15. Cambier J.: Iridian large database performance. Iridian Technologies technical report 03-02, `http://iridiantech.com` (2007)
16. Mansfield T.,Kelly G., Chandler D., Kane J.: Biometric product testing final report. issue 1.0 (2001)
17. Matey J. R., Ackerman D., Bergen J., Tinker M.: Iris recognition in less constrained environments. Springer Advances in Biometrics: Sensors, Algorithms and Systems. 107–131 (2007)
18. Meredith P, Sarna T.: The phisical and chemical properties of eumelanin. Pigment Cell Research, **19**, 572–594 (2006)
19. P. E. Miller P., Rawls A., Pundlik S., Woodard D.: Personal identification using periocular skin texture. In *Proceedings of the ACM* 25^{th} *Symposium on Applied Computing*, ACM Press (2010)

20. Park U., Ross A., Jain A.K.: Periocular biometrics in the visible spectrum: A feasibility study. In *Proceedings of the Biometrics: Theory, Applications and Systems (BTAS 2009) Conference*. 153–158 (2009)
21. Narayanswamy R., Johnson G., Silveira P., Wach H.: Extending the imaging volume for biometric iris recognition. Applied Optics. **44**, 5, 701–712 (2005)
22. Nemati B., H. G. R. III, Welc A. J.: Optical properties of conjunctiva, sclera, and the ciliary body and their consequences for transscleral cyclophotocoagulation. Applied Optics. **35**, 19, 3321–3327 (1996)
23. Park K., Kim J.: A real-time focusing algorithm for iris recognition camera. IEEE Transactions on Systems, Man and Cybernetics. **35**, 3, 441–444 (2005)
24. Proença H., Filipe S., Santos R., Oliveira J., Alexandre, L.: The UBIRIS.v2: A Database of Visible Wavelength Iris Images Captured On-The-Move and At-A-Distance. IEEE Transactions on Pattern Analysis and Machine Intelligence. **32**, 8, 1529–1535 (2010)
25. Ross A., Crihalmeanu S., Hornak L., Schuckers S.: A centralized web-enabled multimodal biometric database. In *Proceedings of the 2004 Biometric Consortium Conference (BCC)*, U.S.A (2004)
26. Smith K., Pauca V. P., Ross A., Torgersen T., King M.: Extended evaluation of simulated wavefront coding technology in iris recognition. In *Proceedings of the First IEEE International Conference on Biometrics: Theory, Applications, and Systems*. 1–7, U.S.A (2007)
27. Viola P., Jones M.: Robust Real-time Face Detection. International Journal of Computer Vision, **57**, 2, 137–154 (2002)
28. Yoon S., Bae K.,Ryoung K., Kim P.: Pan-tilt-zoom based iris image capturing system for unconstrained user environments at a distance. Lecture Notes in Computer Science, **4642**, 653–662, U.S.A (2007).